Science of Remote Sensing 10 (2024) 100176

Contents lists available at ScienceDirect

Science of Remote Sensing

journal homepage: www.sciencedirect.com/journal/science-of-remote-sensing

Coastal vertical land motion across Southeast Asia derived from combining tide gauge and satellite altimetry observations

Dongju Peng [a,b,*], Grace Ng [a,c], Lujia Feng [a,c], Anny Cazenave [d], Emma M. Hill [a,c]

[a] Earth Observatory of Singapore, Nanyang Technological University, Singapore
[b] Department of Land Surveying and Geo-Informatics, The Hong Kong Polytechnic University, Hong Kong Special Administrative Region
[c] Asian School of the Environment, Nanyang Technological University, Singapore
[d] Laboratoire d'Etudes en Géophysique et Océanographie Spatiales, Toulouse, France

ARTICLE INFO

Keywords:
Vertical land motion
Satellite altimetry
Tide gauge
Southeast asia

ABSTRACT

Vertical land motion (VLM) is complex in Southeast Asia because this region is subject to a range of natural processes (e.g., earthquakes) and anthropogenic activities (e.g., groundwater withdrawal) that can change land heights. To aid in coastal management, long-term observations of VLM are as crucial as observations for climate-induced sea surface height changes; however, such long-term observations are sparse for Southeast Asian coasts. To fill this observational gap, here we derive monthly VLM time series from 1993 to 2020 at 50 coastal sites across Southeast Asia by combining tide-gauge records and newly generated satellite altimetry observations. These altimetry observations are reproduced sea-level products using new altimetry standards and more accurate geophysical corrections. Our 27-year-long VLM dataset shows high spatial variability and non-linear temporal changes in VLM across Southeast Asia. We identify several major sources that dominate the regional land-height changes, which include large subsidence due to groundwater extraction in Manila and Bangkok, land uplift in Indonesia and subsidence in Thailand from postseismic deformation resulting from the sequence of large Sumatran earthquakes since 2004, and land subsidence as a result of sediment compaction in Malaysia. Those signals are quantitatively or qualitatively consistent with observations from other sources. This VLM dataset can be used to advance our understanding of the physical mechanisms behind land-height changes and to improve sea level projections in the region.

1. Introduction

Relative sea-level rise is a major threat to coastal zones as it increases the risk of flooding and the salinization of water aquifers and agricultural soil (Becker et al., 2020; Li et al., 2018; Reimann et al., 2018; Vu et al., 2018). Relative sea-level rise can result from a climate-induced increase in sea surface height or a decrease in land height. The former plays the biggest role in global mean sea-level rise, while the latter could exacerbate regional sea-level rise from climate change and may exceed the climate-related contribution in some regions. For example, in the Torres Islands (Vanuatu), vertical land motion (VLM) due to tectonic activities dominates the relative sea-level rise, exceeding the high rate of climate-induced regional sea-level rise (Ballu et al., 2011). The compound effect of sea-level rise due to climate change and land subsidence due to tectonic deformation led to increasing sea incursions, ultimately forcing the displacement of a coastal village in 2002–2004. Therefore, quantifying the contribution of VLM to sea-level rise is as crucial as evaluating the climate change contribution for risk mitigation in low-lying coastal communities, especially for regions that are sinking in the long term. Also, due to its important contribution to relative sea-level rise, VLM and the associated uncertainties must be accounted for in order to generate reliable sea-level projections at regional scales (Arias et al., 2021), which are most relevant for coastal planners and decision makers.

Southeast Asia is extremely vulnerable to relative sea-level rise and coastal flooding as this region is home to 71% of the global coastal population who live within 10 m above sea level and 75% of the global coastal floodplain population (Herrera-García et al., 2021; Nicholls et al., 2021). This vulnerability is worsened by the rapid land subsidence that most major Southeast Asian cities are experiencing (Tay et al., 2022). VLM in Southeast Asia can be caused by natural processes such as tectonic deformation. For example, a sequence of great earthquakes,

* Corresponding author. Earth Observatory of Singapore, Nanyang Technological University, Singapore.
E-mail address: dongju.peng@polyu.edu.hk (D. Peng).

https://doi.org/10.1016/j.srs.2024.100176
Received 6 August 2024; Received in revised form 18 October 2024; Accepted 9 November 2024
Available online 12 November 2024
2666-0172/© 2024 The Authors. Published by Elsevier B.V. This is an open access article under the CC BY-NC-ND license (http://creativecommons.org/licenses/by-nc-nd/4.0/).

with three larger than magnitude 8, were generated by the Sumatran subduction zone in Indonesia since 2004 (Feng et al., 2015). These earthquakes have caused land subsidence or uplift at least 1000 km away from the earthquake sources (Qiu et al., 2018; Satirapod et al., 2013; Simons et al., 2019; Trisirisatayawong et al., 2011). VLM in Southeast Asia can also be changed by anthropogenic activities such as groundwater extraction. Land subsidence due to groundwater extraction has been reported to have reached >10 cm/yr in Jakarta (Indonesia), Bangkok (Thailand), and Manila (The Philippines) (Abidin et al., 2011; Phien-wej et al., 2006; Raucoules et al., 2013; Rodolfo and Siringan, 2006). Excessive groundwater extraction has also been found to be the main driver of land subsidence in the Mekong delta (Vietnam), resulting in the delta sinking an average of ~18 cm from 1991 to 2015 (Minderhoud et al., 2017).

The two most commonly used systems for measuring VLM are the Global Navigation Satellite System (GNSS) and Interferometric Synthetic Aperture Radar (InSAR) (e.g., Hamling et al., 2022; Hammond et al., 2021; Poitevin et al., 2019; Santamaría-Gómez et al., 2012; Shirzaei et al., 2021). GNSS measures land deformation relative to the mass center of the Earth at point locations, whereas InSAR maps ground deformation of swathes of land in the line-of-sight (LOS) direction of a SAR satellite relative to a ground reference point within the SAR scene. GNSS stations in Southeast Asia were installed mostly in the 21st Century (e.g., Din et al., 2019; Feng et al., 2015; Schöne et al., 2011), while InSAR became popular in generating VLM time series only after the second generation of SAR sensors (with a reduced revisit time and an improved spatial resolution) have been operational since 2007 (Sansosti et al., 2014). The most precise VLM measurements are obtained from GNSS, which can reach mm-level precision and have long-term stability, but GNSS stations are limited and most of them are not along the coasts. InSAR can provide global land coverage but InSAR measurements are less precise than GNSS measurements, and InSAR may face technical challenges such as correcting atmospheric disturbances and referencing to a geocentric frame when it comes to deriving long-term (>15 years) VLM time series. However, densely distributed VLM information with long time series are crucial to understanding the non-linearity of VLM due to the regional complexity of physical processes (Featherstone et al., 2015; Oelsmann et al., 2024; Raucoules et al., 2013) and the spatial variation of VLM at small scales (Hammond et al., 2021; Pfeffer and Allemand, 2016). To help provide such a dataset, in this study we combine long-term tide-gauge observations with satellite altimetry measurements that provide absolute (geocentric) sea level values, to derive VLM along the coasts of Southeast Asia. VLM information from this method can date back to August 1992 when the first high-precision satellite mission (i.e., TOPEX/Poseidon) that was specifically designed to monitor sea surface height began to collect data. The VLM information from combining tide gauge and satellite altimetry can complement GNSS and InSAR measurements to increase the spatial and temporal coverage of VLM observations and they can be used to constrain physics based VLM models in the region (e.g., Rezvani et al., 2024).

Satellite altimetry measures geocentric sea level relative to the center of the Earth (N), whereas tide gauges measure changes in sea level relative to the land (S) where they are located (Fig. 1), including changes in both geocentric sea level (N) and land height (U). Assuming that satellite altimetry and tide gauges capture the same changes in geocentric sea level, differencing observations from the two observing systems can generate VLM changes ($U = N - S$) at tide-gauge sites. This method was first introduced by Cazenave et al. (1999) and has since been applied to numerous regions worldwide to obtain VLM at tide-gauge sites (e.g., De Biasio et al., 2020; Fadil et al., 2013; Iz et al., 2020; Kuo et al., 2004; Rezvani et al., 2022; Watson, 2019; Wöppelmann and Marcos, 2012).

Ideally, satellite altimetry measurements should be nearby tide-gauge sites for deriving reliable VLM information, because sea-level trends near the coast might differ from those in the open ocean (Cazenave et al., 2022). However, conventional satellite altimetry products are not reliable within 10–15 km of the coast due to the contamination of altimetric waveforms from the land and/or inadequate geophysical corrections (Benveniste et al., 2020). With recent advances in satellite altimetry techniques, two new satellite altimetry products are now available for Southeast Asia: the first one is a global conventional gridded dataset with improved data quality by using new altimetry standards and more accurate geophysical corrections (Taburet et al., 2019), and the second one is a dedicated coastal along-track altimetry dataset specifically for the Southeast Asian region (Benveniste et al., 2020). Previous studies used the older version of the gridded satellite altimetry products to derive VLM in the region, covering time periods only up to 2011. Examples include Fenoglio-Marc et al. (2012) for Indonesia, Din et al. (2019) for Malaysia, and Trisirisatayawong et al. (2011) for Thailand. With longer and more accurate altimetry-based sea-level data available, our goal is to revisit this method for deriving long-term VLM time series. VLM from this method can complement the spatiotemporal gaps in GNSS and InSAR measurements in the region, potentially leading to a better understanding of the underlying physical mechanisms and enhancing regional sea-level projections. To achieve this goal, we first validate the new along-track sea-level products, and then assess the effectiveness of the two new sea-level products in generating VLM through comparison with nearby GNSS observations. Finally, we investigate the major factors responsible for changes in land heights.

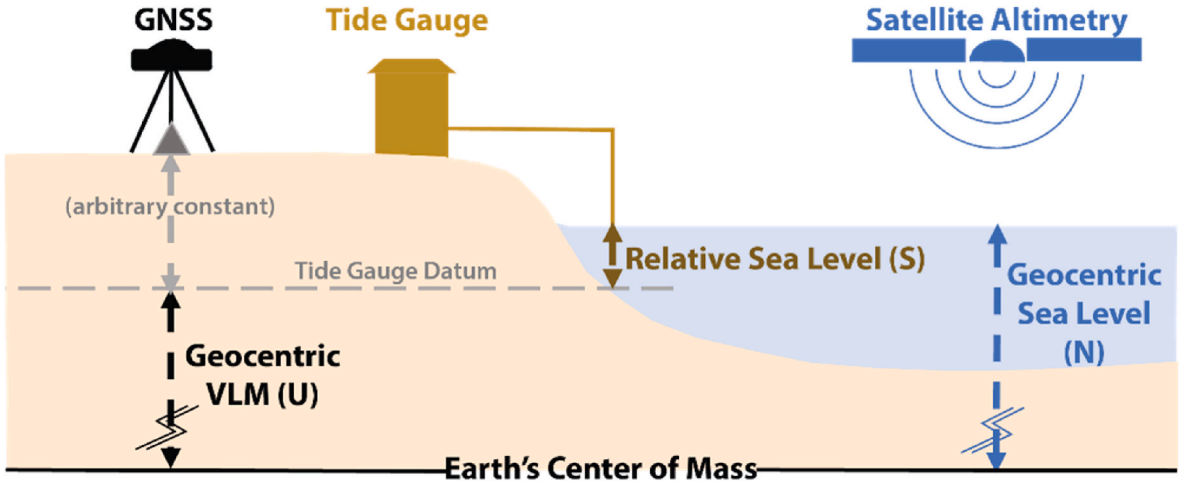

Fig. 1. Schematic of satellite altimetry, tide gauge and GNSS measurements. Modified from Wöppelmann and Marcos (2016). VLM at a tide-gauge site can be determined by incorporating geocentric sea level measurements from satellite altimetry to account for changes in sea surface height in the tide-gauge records.

The manuscript is organized as follows: Section 2 presents the data and methodology employed to derive VLM. Section 3 evaluates the performance of the new along-track sea-level products. Section 4 compares the VLM derived from the along-track and gridded sea-level products in five scenarios at tide-gauge sites with nearby GNSS stations. Section 5 assesses the quality of VLM estimates generated from the most effective scenario compared to GNSS observations in Section 4 across all 50 sites. Finally, Section 6 identifies several major sources of land-height changes in the region.

2. Data and methods

2.1. Data

To quantify the VLM in Southeast Asia, we used three types of data: (1) tide-gauge records, (2) satellite altimetry data, and (3) GNSS vertical measurements. We selected 50 regional tide gauges with record length >10 years during 1993–2020, and six of them with a GNSS station at a distance <10 km (Fig. 2). We used monthly tide gauge data from the archives of the Permanent Service for Mean Sea Level (PSMSL) (Holgate et al., 2013) and daily GNSS vertical measurements produced by the Nevada Geodetic Laboratory (Blewitt et al., 2018). For satellite altimetry data, we adopted two different sea level products: (1) gridded sea-level anomalies (SLA) produced by the Copernicus Climate Change Service (Taburet et al., 2019) and (2) coastal along-track SLA produced by the Climate Change Initiative Coastal Sea Level Team (Benveniste et al., 2020). The gridded products are reprocessed multi-mission altimetric solutions with daily temporal resolution and spatial sampling of 0.25°. The coastal along-track sea level products (computed in the context of the Climate Change Initiative (CCI) coastal sea level project of the European Space agency/ESA) were derived with a complete reprocessing of Jason-1, 2 and 3 altimetry data over January 2002 to May 2018. The reprocessing involves: (1) employing an adaptive leading edge sub-waveform retracking method to estimate the altimeter range from waveforms collected in coastal zones, (2) utilizing enhanced geophysical corrections for atmospheric effects (wet and dry troposphere, ionosphere, inverse barometer), geophysical phenomena (ocean tides, high frequency atmospheric effects on the ocean) and the sea-surface state

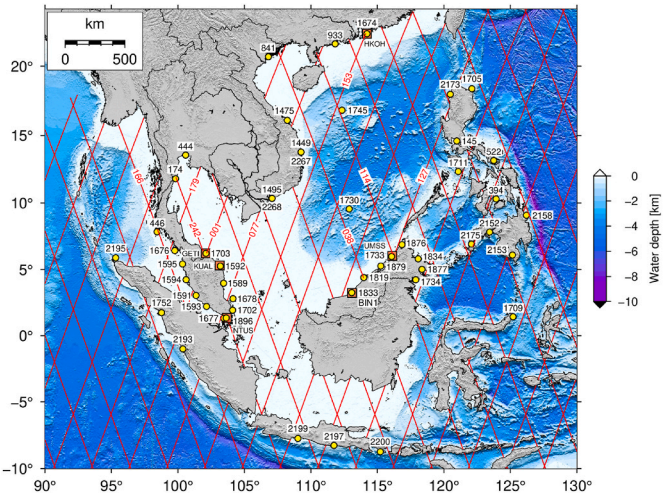

Fig. 2. Location map of tide gauges (yellow dots), GNSS stations (orange squares) and tracks of Jason satellites (red lines). The tide gauges are owned by Indonesia (2195, 1752, 2193, 2199, 2197, 2200, 1709), Thailand (446 174, 444), Malaysia (1676, 1595, 1594, 1591, 1591, 1677, 1702, 1678, 1589, 1592, 1703, 1833, 1819, 1879, 1733, 1876, 1834, 1877, 1734), Singapore (1896), Vietnam (1495, 2268, 2267, 1449, 1475, 841), The Philippines (2173, 1705, 145, 1711, 522, 394, 2175, 2152, 2158, 2153) and China (1730, 1745, 933, 1674). (For interpretation of the references to color in this figure legend, the reader is referred to the Web version of this article.)

(electromagnetic sea-surface bias), and (3) implementing a rigorous data editing procedure tailored to coastal ocean conditions. Further details on the data processing are available in Benveniste et al. (2020), Birol et al. (2021) and Cazenave et al. (2022). This product provides along-track, high-resolution (20 Hz, i.e., ~350 m) SLA at 10-day intervals and reaching to within 15 km of the coast (i.e., largely covering the coastal gap in the gridded products).

2.2. Methods

Fig. 3 is a flowchart showing how we derived VLM from a combination of satellite altimetry and tide-gauge observations. We note that SLA from satellite altimetry products contain only oceanic signals because the dynamic atmospheric corrections (DAC) that account for variations in sea level due to low-frequency inverse barometer response and high-frequency wind and pressure effects (Carrère et al., 2003) were removed in both along-track and gridded products. First, therefore, we removed the DAC time series from the tide-gauge data, since those raw data include both oceanic and atmospheric signals. To be consistent, we used the same DAC products that had been applied to the altimetry data, with a temporal resolution of 6 h and spatial sampling of 0.25°. For each site we first extracted the DAC time series from the nearest grid point to the site and averaged the 6-hourly solutions over each month. We then subtracted the monthly DAC from the tide-gauge data to remove the atmospheric effects.

Secondly, we removed seasonal signals and a linear rate in both satellite altimetry data and tide-gauge records to obtain the inter-annual variability of sea level. We first averaged both gridded and along-tack SLA data on a monthly basis to form monthly SLA time series from satellite altimetry. We then fit the monthly sea-level data ($y(t)$) with a model including annual and semi-annual harmonics, a linear rate and an offset as below:

$$y(t) = a + bt + c_1 \sin(2\pi t) + c_2 \cos(2\pi t) + d_1 \sin(4\pi t) + d_2 \cos(4\pi t) + \varepsilon(t)$$

where, t represents time. a is an offset, b is a linear rate, $c_1 \sin(2\pi t) + c_2 \cos(2\pi t)$ and $d_1 \sin(4\pi t) + d_2 \cos(4\pi t)$ denote annual and semi-annual signals, respectively. ε is inter-annual variability plus data noise. The data noises of tide-gauge and satellite altimetry measurements are at mm level and 1–2 cm level, respectively. They are negligible compared with the inter-annual variability of sea level, that is on the order of >10 cm. Thus, we assumed that ε represents inter-annual sea-level variability. We calculated two types of time series for both satellite altimetry (N) and tide-gauge (S) data: (a) inter-annual variability of sea level (N_a, S_a), i.e., with a linear rate and seasonal signals removed, for calculation of correlation coefficients (CC) and (b) inter-annual variability of sea level plus a linear rate (N_b, S_b), i.e., with seasonal signals removed, for calculation of VLM.

Thirdly, we selected the satellite altimetry measurements that best represent the ocean signals captured by tide gauges. We considered five scenarios: (S_1) the closest along-track point to a tide gauge (Watson, 2019), (S_2) the best correlated along-track point (Santamaría-Gómez et al., 2014), (S_3) the along-track zone of influence (ZOI) (Oelsmann et al., 2021), (S_4) the best correlated gridded point, and (S_5) the gridded ZOI. The best correlated point represents the point that exhibits the highest CC within 100 km distance from a tide gauge. The CC are calculated using the inter-annual variability of sea levels from satellite altimetry (N_a) and tide gauges (S_a). The ZOI is restricted to the 20% best data within 100 km to a tide gauge in terms of CC; we averaged the 20% data to represent the ZOI time series.

Lastly, we formed VLM time series at tide-gauge sites using the selected satellite altimetry data. Here, the time series with seasonal signals removed were used, i.e., $U = N_b - S_b$. We also calculated linear rates and the associated uncertainties of VLM from selected sites (see Section 5 for details). For each selected VLM time series, we first

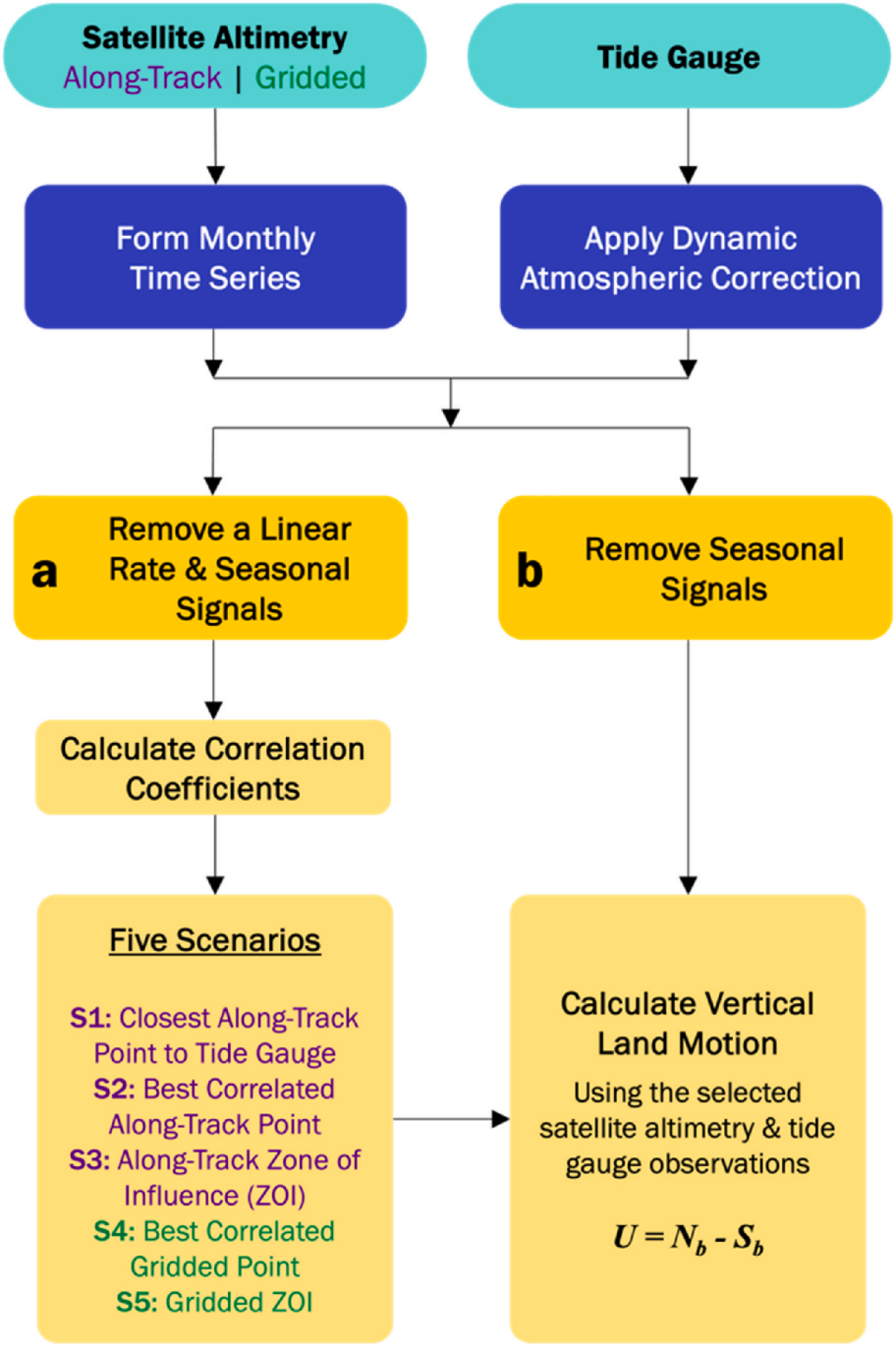

Fig. 3. Flowchart of the procedures applied to drive VLM from satellite altimetry and tide gauge observations.

computed detrended time series and removed outliers located outside a 2-σ threshold around the root mean squares of the detrended time series (Benveniste et al., 2020). We then re-calculated the linear trend and its associated uncertainty (1-σ) of the edited VLM time series using the Senales y Analisis de Ruido Interactivo (Interactive Signal and Noise Analysis; SARI) software (Santamaría-Gómez, 2019) and a combination of a power-law and a white noise model. SARI is an online tool for interactive time series processing and allows estimation of uncertainties based on a combination of a colored noise model and a white noise model. It is important to note that sea level undergoes decadal variations, such as the 18.6-year lunar nodal cycle (Bult et al., 2024; Peng et al., 2019). Depending on the geographic location, further mitigation of these periodic signals may be necessary for a robust estimation of VLM trends. For consistency, we applied the same procedure and noise model to the GNSS time series to determine the trend of VLM.

3. Validation of the along-track CCI coastal sea level products in southeast asia

To achieve the goals of this study we need to examine whether the closest points of the along-track altimetry observations can provide better estimations of VLM than the best-correlated points of along-track and gridded products. Given that along-track CCI coastal sea level data in Southeast Asia are new, we first validate the data in terms of both the closest points and the best correlated points by adopting the approach proposed by Dieng et al. (2021). Their approach was used to validate the along-track CCI coastal sea-level products in the Mediterranean Sea.

Following Dieng et al. (2021) and also to reduce the effects of small-scale errors on the altimetry observations, we averaged the data every 2 km from the first valid measurement in the offshore direction (data completeness >75%; see Fig. 4) and converted the data into monthly data. In contrast, the daily gridded SLA were generated by an optimal interpolation technique with a centered computation time window of ±6 weeks around the computation time (Taburet et al., 2019). They are essentially an average of the SLA over 12 weeks. To be consistent with the gridded data and to further reduce data noise, we applied a filter of a 3-month moving average to the monthly along-track SLA data. Seasonal (annual and semi-annual) signals and a linear trend were removed to obtain inter-annual variability for the calculation of CC and root-mean-square deviation (RMSD) between satellite altimetry and tide-gauge time series. Fig. 5 shows the inter-annual variability of sea level from tide gauge site 1733 and satellite altimetry track 114. For this track, the closest valid along-track point is 3.1 km to the coast and 24.1 km to the tide gauge. As anticipated, the best correlated point shows higher CC and lower RMSD than the closest point.

We considered only those satellite tracks in the study region located within 30 km of a tide gauge, i.e., the distance between the first valid point and a tide gauge is < 30 km. This led us to keep only 10 track portions. Table 1 summarizes the CC and RMSD between tide-gauge records and altimetry-based sea levels from the five scenarios, and the corresponding distances to tide gauges. Among the distances, S_0 denotes the distance of the first valid along-track point to the coast. In general, the closest along-track points (S_1) exhibit the largest RMSD and lowest CC among the five scenarios. This is consistent with the findings in the Mediterranean Sea: gridded SLA have larger correlation coefficients and smaller RMSD with tide-gauge data than the coastal along-track SLA (Dieng et al., 2021), likely reflecting a larger noise level in the coastal along-track data.

Table 1 also shows that the best correlated gridded points (S_4) outperform the best correlated along-track points (S_2) in terms of both RMSD and CC, except for site 1745 where the best correlated along-track point (S_2) has slightly lower RMSD and higher CC than the best correlated gridded points (S_4). Since gridded SLA are essentially interpolated temporally and spatially from along-track observations, the along-track observations may have better agreement with tide-gauge observations when they are in ideal observational conditions. Site 1745 is located on a small island in the middle of the sea (Fig. 1), and the CC of the best correlated along-track observation point reached 0.93. This suggests that the observational circumstances around this location are more conducive to satellite altimetry than the coastal zones. As a result, the along-track observations at this site better agree with the nearby tide gauge than those at the coastal zones. Additionally, the ZOI scenarios appear to be similar to the best-correlated scenarios for both along-track and gridded altimetry SLA.

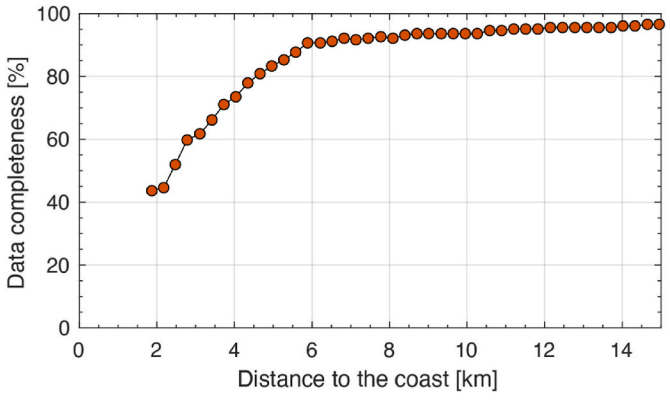

Fig. 4. Data completeness within 15 km to the coast from track 038. The closest point to the coast is < 2 km, but the data completeness is <75%. The first valid point with data completeness >75% is at around 4.3 km to the coast.

For the closest along-track points (S_1), poor agreement between altimetry and tide-gauge time series are found at half of the sites, where the CCs are <0.5 and the largest RMSD reaches 7.5 cm. In comparison, the CCs at 12 sites out of 14 sites in the Mediterranean Sea are >0.5 and the corresponding RMSDs are <4.6 cm (Dieng et al., 2021). This suggests that the data quality of the first valid points from the along-track CCI data in Southeast Asia may still be further improved. We note satisfactory agreement between the best correlated altimetry-based time series (both along-track and gridded) and tide-gauge time series, with the CCs >0.5 for all the selected along-track time series. The CCs for the gridded time series are even higher (>0.7 for all the sites). The RMSDs for best correlated points (both along-track and gridded) at all sites except site 1745 are lower than those for the closest along-track points. In addition, the RMSDs for the best correlated gridded points are <4 cm, except at site 446. A closer look reveals that site 446 is located in a bay area in Thailand near the Bay of Bengal, where the inter-annual variability of sea level is greatly affected by the Indian monsoon winds (Han and Webster, 2002; Sreenivas et al., 2012). The monsoon effect is likely responsible for the larger RMSD as the effect on sea level is not uniform across the region, and the gridded point of satellite altimetry and the tide gauge are ~94 km apart.

4. Validation of VLM estimates with GNSS observations

We use GNSS observations to validate the VLM time series derived from satellite altimetry and tide gauges. There are six tide-gauge sites with a GNSS station at <10 km distance, namely 1733 (UMSS, 7.9 km), 1833 (BIN1, 4.2 km), 1592 (KUAL, 7.9 km), 1703 (GETI, 0.2 km), 1674 (HKOH, 5 km; HKQT, co-located), and 1896 (NTUS, 5.2 km). Among those, 1733, 1674, 1703 and 1896 are at distances <30 km from the Jason tracks. For site 1674, we compared the vertical positions of HKQT and HKOH over their common time periods (2008–2022) and found that they are similar. Therefore, we chose HKOH to validate the VLM at 1674 as it has three more years of observations than HKQT.

Compared with the other three sites that are close to the Jason tracks, site 1733 has the highest CC for the first valid along-track SLA time series. We display the corresponding VLM time series from the five scenarios and GNSS in Fig. 6. GNSS time series were corrected for an offset of 2.1 cm on June 4, 2015, due to a magnitude 6.0 earthquake at a distance of 48 km away from the station. S_4 and S_5 (gridded SLA) scenarios show the land was uplifting and became subsiding from 2006 onwards. Along-track SLA (S_1, S_2, S_3 scenarios) and GNSS data are too short to capture the changing behavior of the land. Investigation of the reasons causing the direction change of land movement is beyond the scope of the study. For consistency and validation purposes, we calculated linear trends of VLM and GNSS time series over their common time periods (i.e., 2007–2019). Fig. 7a shows the linear rates and the associated uncertainties for this site. As expected, uncertainties involving along-track data are larger than those using conventional gridded altimetry data, and the largest uncertainty comes from S_1. The linear trends from the best correlated and ZOI time series of along-track (S_2 and S_3) and gridded (S_4 and S_5) products are generally in good agreement with GNSS rates; however, the scenario of the closest along-track point (S_1) overestimate the VLM rate at this site (almost two times the linear rate from best correlated point). Given that the closest along-track time series has high CC and low RMSD with tide-gauge time series, this may suggest that coastal SLA data capture some local oceanic signal not active offshore nor seen by the tide gauge (which is in general located in sheltered zones at the coast).

We summarize the linear trends and uncertainties for the rest of the five sites in Fig. 7. Generally, the uncertainties for the remaining sites exhibit similar characteristics to site 1733: VLM from along-track data tends to have greater uncertainties compared to gridded data. One possible cause of this discrepancy could be the imprecision of the along-track data. Linear trends of VLM from the five scenarios and GNSS were calculated over common time periods. We also display the VLM time

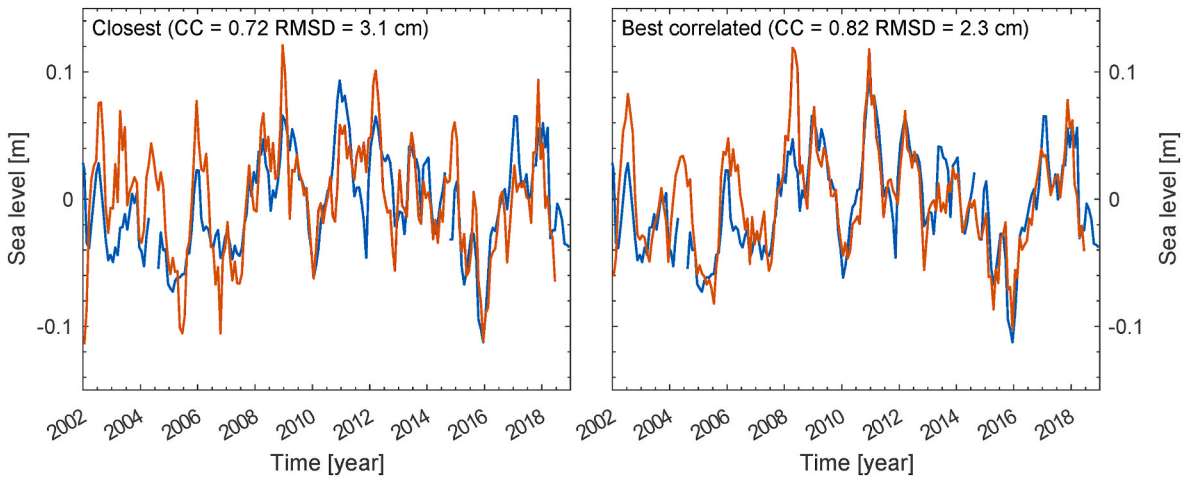

Fig. 5. Inter-annual sea levels from tide gauge (1733) and along-track satellite altimetry (closest point and best correlated point). Blue line indicates tide gauge, whereas red line indicates satellite altimetry. (For interpretation of the references to color in this figure legend, the reader is referred to the Web version of this article.)

Table 1
CC and RMSD differences between altimetry and tide-gauge time series.

Site/track	Distance (km)				CC					RMSD (cm)				
	S_0	S_1	S_2	S_4	S_1	S_2	S_3	S_4	S_5	S_1	S_2	S_3	S_4	S_5
1733/114	3.1	24.1	91.7	74.1	0.73	0.82	0.84	0.93	0.93	3.0	2.4	2.2	1.9	1.9
1677/077	8.0	22.1	32.1	204.9	0.42	0.53	0.53	0.78	0.78	4.4	4.1	4.1	3.2	3.2
446/166	2.7	9.8	83.1	93.9	0.45	0.54	0.54	0.76	0.76	6.5	5.9	5.9	5.3	5.3
1703/001	4.0	7.2	72.7	71.8	0.53	0.72	0.73	0.84	0.85	4.5	2.7	2.7	2.9	2.9
174/242	4.3	7.6	56.5	99.9	0.40	0.51	0.51	0.75	0.75	4.3	3.6	3.6	3.4	3.4
1745/114	21.0	22.1	49.7	6.4	0.79	0.93	0.94	0.90	0.89	3.7	2.3	2.0	3.1	3.3
1674/153	1.8	12.6	57.4	98.0	0.53	0.69	0.70	0.81	0.82	6.1	3.4	3.4	3.7	3.6
1746/242	2.4	16.0	66.9	94.9	0.36	0.57	0.56	0.79	0.77	6.7	3.3	3.2	2.4	2.5
1351/242	1.8	1.8	63.3	97.5	0.35	0.58	0.59	0.75	0.73	7.5	3.4	3.3	2.7	2.8
1896/242	2.4	26.5	86.4	89.9	0.52	0.53	0.56	0.79	0.77	6.3	3.6	3.5	3.2	3.2

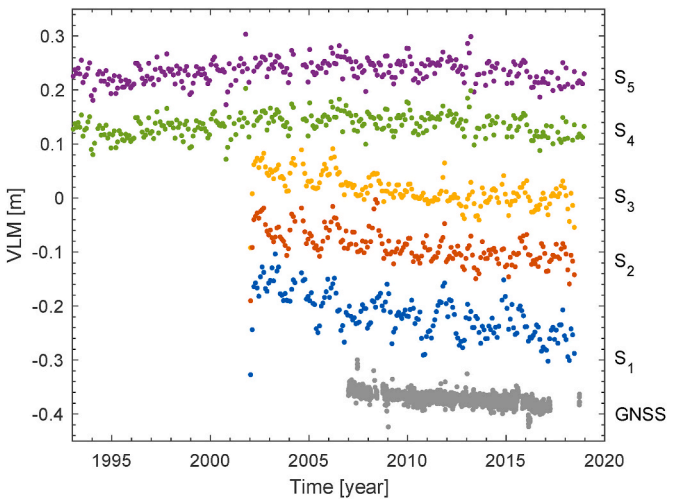

Fig. 6. VLM time series (colored dots) for the five scenarios (S_1: the closest along-track point to a tide gauge; S_2: the best correlated along-track point; S_3: the along-track ZOI; S_4: the best correlated gridded point; S_5: the gridded ZOI) from 1733 tide gauge and UMSS GNSS (grey dots).

series from the best correlated gridded points (S_4) for the six sites superimposed with the GNSS time series in Fig. 8. For site 1592, there were only a few GNSS observations before 2007, so we calculated linear trends from 2007 to 2018. For site 1703, a change of sign of land movement (i.e., uplift before ~2006 and subsidence afterward) is observed in both GNSS and VLM time series. Considering record lengths and data gaps, we used GNSS data only after 2007. Also, the GNSS vertical positions become noisier after 2014 (i.e., years 2014 and 2015); for consistency, we removed data for years 2014 and 2015 when calculating linear trends (i.e., linear trends for site 1703 shown in Fig. 7 were calculated over years 2007–2014).

Fig. 7 shows that the linear trends from the best correlated points (S_4 and S_2) are in better agreement with GNSS rates than the rest of the scenarios. No significant improvement was found by using ZOI (S_3 vs S_2 and S_5 vs S_4). Also, S_1 appears to overestimate the trends. Besides data imprecision, this may indicate the presence of coastal small-scale processes in the region, which will result in a coastal modification in the character of the large-scale sea level variability. The six sites are all located in shallow continental shelf areas (water depth <300 m), which favor small-scale processes (Woodworth et al., 2019). Tide gauges are usually located in protected harbors, where small-scale coastal processes (e.g., wave breaking) are limited. It is possible that the inter-annual variabilities of sea level in the tide-gauge data are from the large-scale oceanic causes (e.g., El Niño-Southern Oscillation). If that is the case, best correlated offshore satellite altimetry observations better represent the inter-annual sea-level variability recorded by tide gauges than coastal satellite altimetry observations, thus better meeting the assumption that tide gauges and satellite altimetry capture the same oceanic signals.

5. Data quality of VLM derived from the best correlated gridded point

Comparison with GNSS observations (Section 4) demonstrated that

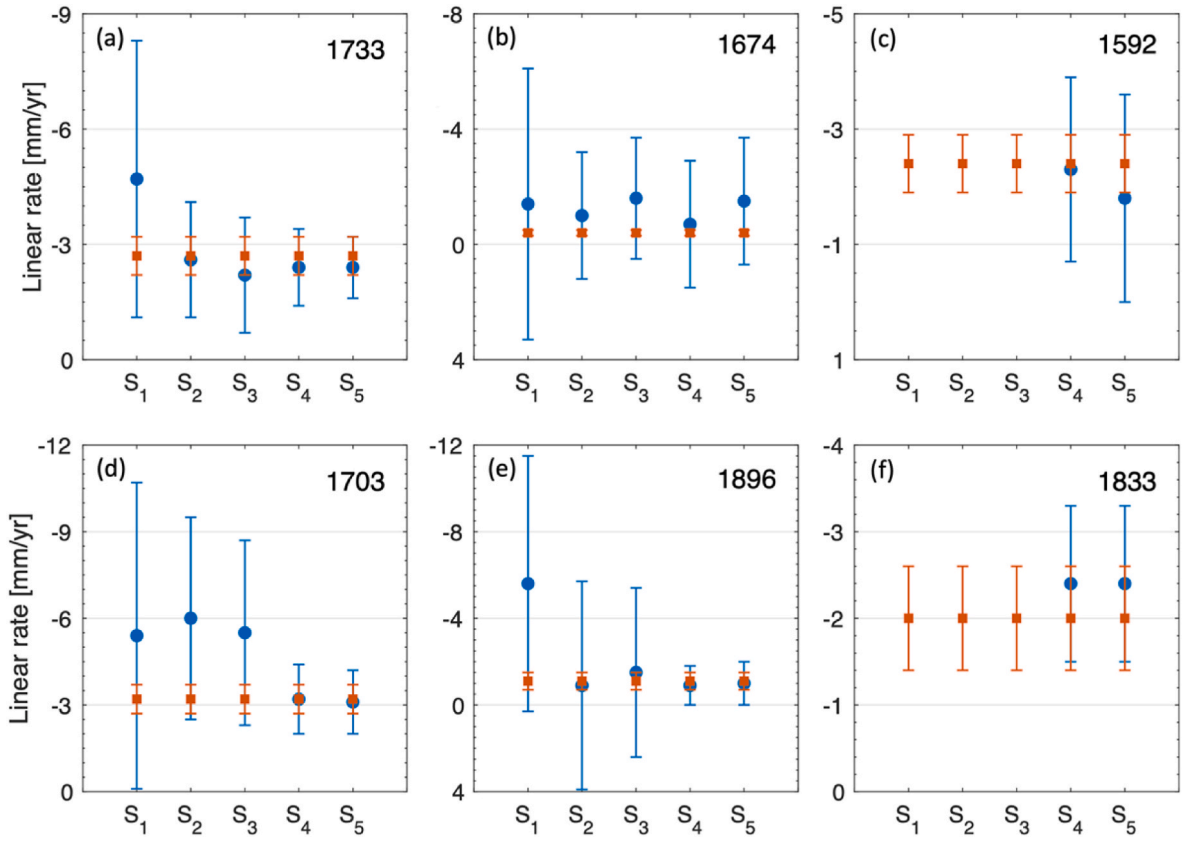

Fig. 7. Linear rates and associated uncertainties for the six tide gauges with GNSS stations nearby. Blue circles represent the linear rates from the five scenarios, and red rectangles represent linear rates derived from GNSS vertical measurements. (For interpretation of the references to color in this figure legend, the reader is referred to the Web version of this article.)

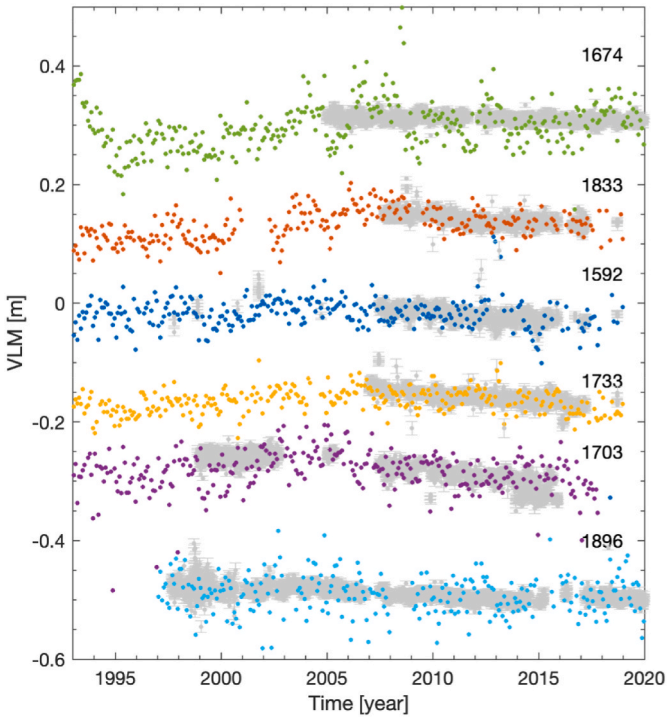

Fig. 8. VLM time seires derived from satellite altimetry and tide gauge observations (colored dots) superimposed with GNSS time series (grey dots).

the best correlated gridded satellite altimetry points (S_4) outperform the other four scenarios, which is consistent with the findings of Oelsmann et al. (2021). They examined VLM at 58 tide gauges derived from gridded satellite altimetry and coastal along-track altimetry and found - by comparing the VLM rates with GNSS observations (located within 1 km to tide gauges) - that the use of a gridded product outperforms the along-track CCI coastal sea level performances. We, therefore, selected the best correlated grid points to calculate VLM for the remaining tide gauge sites. Note that there is a potential limitation in the VLM from this method, as it assumes that any residual altimeter-specific systematic error or bias/drift is negligible, given that global and regional inter-mission biases or drifts are removed in the gridded sea-level time series (Taburet et al., 2019). More details about the altimeter-specific systematic error and their impact on VLM are available in Watson et al. (2015) and Rezvani et al. (2022).

We first examine the CC and RMSD for the best correlated gridded satellite altimetry points. Fig. 9 shows that CCs are all >0.5, with 90% (45 out of 50) > 0.7, suggesting good agreement between the tide gauge and satellite altimetry time series. RMSDs at most of the sites (39 out of 50) are <4 cm. In general, high CC corresponds to low RMSD. We also note high CC and low RMSD in Malaysia and Indonesia. The majority of the sites with RMSD >4 cm (8 out of 10) are in the Philippines. Possible reasons could be (1) the Philippines are an archipelagic country, meaning that altimetric waves are easily contaminated by land, and (2) local ocean dynamics are highly variable both spatially and temporally around the Luzon Strait (where sites 2173 and 1705 are located) due to the Kuroshio intrusion (Nan et al., 2015). Offshore features of SLA may not be fully captured by the sheltered tide gauges, which may cause large discrepancies between tide-gauge data and offshore satellite altimetry observations. RMSDs at two sites in Thailand (446 and 444) are also >4 cm. Possible causes of large RMSD at site 446 were discussed

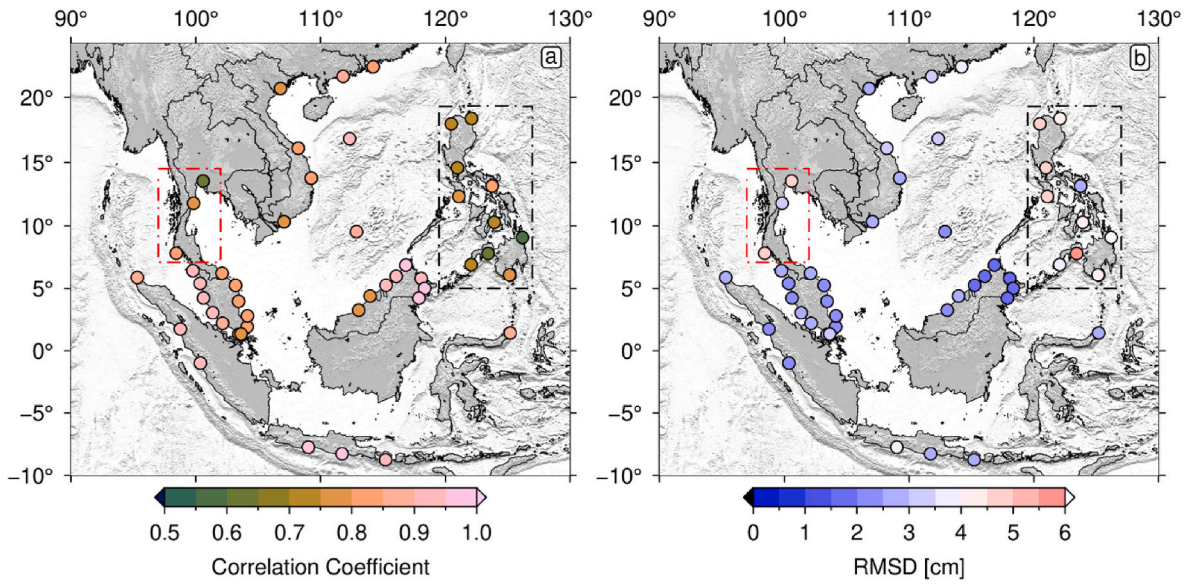

Fig. 9. CC and RMSD between gridded satellite altimetry time series and tide gauge data. Tide gauges in black and red rectangles are in the Philippines and Thailand, respectively. High RMSD and low CC were identified in the two regions within the rectangles. (For interpretation of the references to color in this figure legend, the reader is referred to the Web version of this article.)

in Section 3. As for site 444, it is located at the estuary of Chao Phraya River (the major river in Thailand). It has been known that freshwater runoff from rivers contributes to signals of the order of centimeters in sea level variability on daily timescales for some rivers in Europe, with plumes extending ~10 km from the river mouth (Woodworth et al., 2019). The daily signals from river runoff will inevitably contribute to sea-level variability on seasonal and even inter-annual timescales. Therefore, there is a possibility that inter-annual sea-level variability in the tide-gauge data at site 444 contains signals from river runoff, but offshore satellite altimetry observations do not. Consequently, larger differences between the two types of measurements are observed.

6. Significant signals identified in the VLM time series

VLM signals in the region have high spatiotemporal variability (Figs. S1–S3 showing VLM time series for the 50 sites are in the Appendix). It is not possible to characterize the VLM across the region with one common spatiotemporal pattern. Here, we identify a few major causes responsible for the land-height changes in the region. There may be other causes that contribute to the changes in the land height (e.g., glacial isostatic adjustment), but investigation of the exact driving mechanisms and their contributions to VLM is beyond the scope of this study.

6.1. Groundwater withdrawal

Subsidence resulting from the extraction of groundwater is a well-known issue in major cities in Southeast Asia such as Manila (the Philippines) and Bangkok (Thailand). Our results from tide-gauge records and best correlated satellite altimetry gridded point data (Fig. 10a) show that tide gauge site 145 (located at Manila Bay in the Philippines) has been subsiding at a rate of −9.3 ± 1.9 mm/yr over the period of 1993–2020, which is consistent with InSAR observations (Raucoules et al., 2013). Raucoules et al. (2013) revealed a VLM rate of −8.0 ± 2.0 mm/yr over the period of 2003–2010 at this tide gauge site by analyzing InSAR measurements and linking the LOS rates to a geocentric reference frame.

We observe changes in the rate of subsidence at tide gauge site 444 (located in Bangkok, Thailand) (Fig. 10b). The subsidence slowed down considerably after 2000; the land was subsiding at a rate of −21.7 ± 4.1

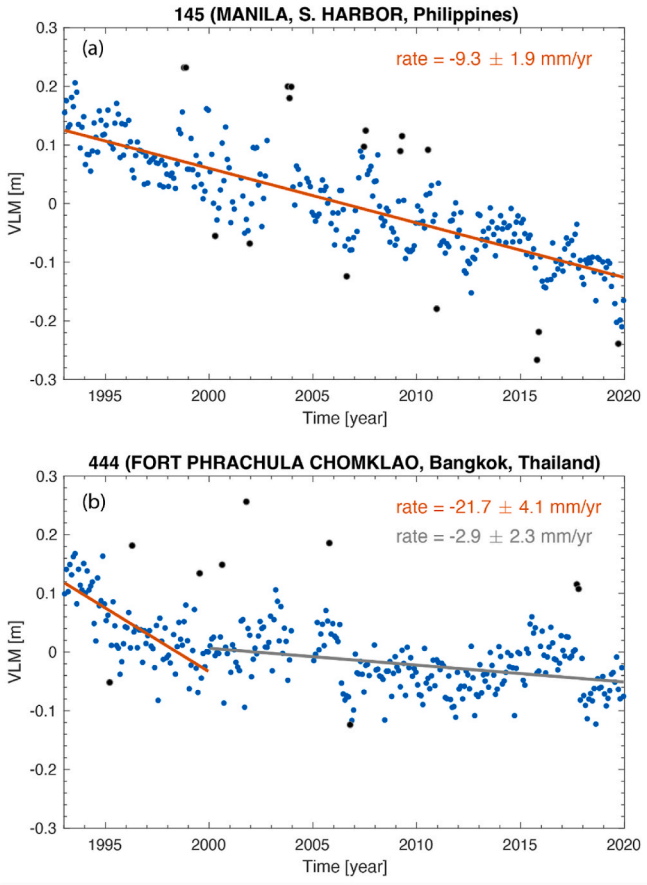

Fig. 10. VLM time series (blue dots) generated from best correlated gridded point at sites 145(a) and 444 (b). Red line in (a) is a linear fit of the blue dots over 1993–2020. Red and grey lines in (b) are a linear fit of the blue dots over the periods of 1993–2001 and 2001–2020, respectively. Black dots are outliers. (For interpretation of the references to color in this figure legend, the reader is referred to the Web version of this article.)

mm/yr from 1993 to 2000 and the rate significantly reduced to −2.9 ± 2.3 mm/yr from 2000 to 2020. This can be primarily attributed to the mitigation measures implemented to regulate and reduce groundwater use in Bangkok Metropolis. It has been reported that the pumping rate increased rapidly after 1993 following a new wave of economic growth and considerably dropped around 2000–2001 because of a pricing policy on groundwater, expansion of tap water supply, and a ban on groundwater use in areas with an accessible tap water supply (Phien-wej et al., 2006). It should be noted that the VLM time series from 2000 to 2020 are not linear; we calculated a linear rate simply for comparison with the rate before 2000 to demonstrate the extraordinary change. Also, although groundwater withdrawal likely plays the primary role, there might be other geophysical signals (e.g., tectonic signals), oceanic signals between the tide gauge and gridded point of satellite altimetry (Rezvani et al., 2022), residual altimeter-specific systematic errors (Rezvani et al., 2021) and tide-gauge datum errors in the VLM time series.

6.2. Tectonics

Southeast Asia has highly diverse seismic hazards, from high seismic hazard associated with the subduction processes beneath the Indonesian and Philippine archipelagos to moderately low seismic hazard across a large stable region that contains the Malaysian peninsula (Petersen et al., 2007). According to the USGS (United States Geological Survey) database, Southeast Asia has witnessed more than 160 large earthquakes with magnitude greater than 6.0 over the past 50 years. Hence, tectonic processes greatly influence the land motions in the region.

Here, we present the VLM time series for five selected sites that show strong signals from tectonic deformations and qualitatively compare them with other sources of measurements. We have another manuscript in preparation which aims to identify all the tectonic signals in this dataset and to examine the tectonic contributions to land-height changes in the region by combining this dataset with GNSS observations and models. We observe land uplift (e.g., sites 2195 and 1752) and land subsidence (e.g., sites 1676, 446 and 174) due to the postseismic processes of large Sumatran earthquakes (notably the 2004 M_w 9.1 Indian Ocean and 2005 M_w 8.6 Nias-Simeulue events) (Fig. 11). The observed pattern is consistent with observations from coral and GNSS (Satirapod et al., 2013; Simons et al., 2019) and numerical models (Qiu et al., 2018) that revealed the near-field (where sites 1752, 2195, etc. are located) land uplift and far-field (where sites 446, 1676, 174, etc. are located) land subsidence. Additionally, Trisirisatayawong et al. (2011) found that two campaign GNSS stations in Thailand uplifted before 2005 and attributed the uplifts to interseismic processes. We also note land uplift in Thailand (e.g., site 174) before 2005, consistent with GNSS observations.

6.3. Sediment accretion and compaction

To adapt to rising sea levels and to minimize coastal erosion, one of the coastal management strategies in Malaysia is to build breakwater structures along river estuaries and coastal beaches to increase coastal accretion (Mohamed Rashidi et al., 2021). As a result of this adaptation measure and the natural process of sediment delivery at a river estuary, 723 acres of shoreline were accreted along the Miri River mouth over the period of 1963–2014 (Anandkumar et al., 2019).

Tide gauge site 1819 is located at the Miri River mouth, and we observe land subsidence at a rate of −3.8 ± 0.7 mm/yr from 1993 to 2016 (Fig. 12). To figure out whether the observed subsidence is a widespread or localized signal, we compare the VLM time series at site 1819 with the two sites 1833 and 1879 which are on the same coastline of Borneo, Malaysia, but are at around 200 km to the south and north of site 1819, respectively (see geographical locations in Fig. 1). VLM time series at sites 1833 and 1879 exhibit similar temporal pattern (Fig. 12), with land uplift before 2005 and land subsidence afterward. Tectonics could potentially play a role in the land-height changes before and after 2005 at these two sites, as discussed in the previous section. In contrast, the VLM time series at site 1819 indicates subsidence. Although the data gap makes the interpretation difficult, subsidence can be noted at this site before 1998. Meanwhile, during the same period, land lift was observed at the other two sites. This suggests that in addition to any regional factors (e.g., tectonics, altimeter-specific systematic errors, etc.), land-height changes at site 1819 were likely influenced by localized factors as well.

According to the geological map in Malaysia, sites 1833 and 1879 are located in areas with extensive sandstones, mudstones, and shale formations, whereas site 1819 is on an alluvial substrate (Hutchison, 2005). Therefore, site 1819 is prone to subsidence from the compaction of unconsolidated sediment. Sediment compaction is often a dominant factor resulting in subsidence in major river deltas (Shirzaei et al.,

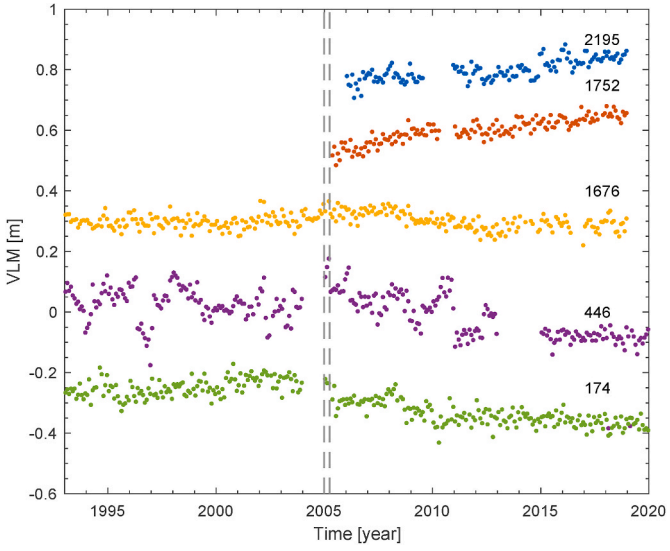

Fig. 11. VLM time series for selected sites where tectonic signals were identified. The two grey dashed lines indicate the two major earthquakes that occurred in Sumatra, Indonesia on December 26, 2004 (magnitude 9.1) and March 28, 2005 (magnitude 8.6), respectively.

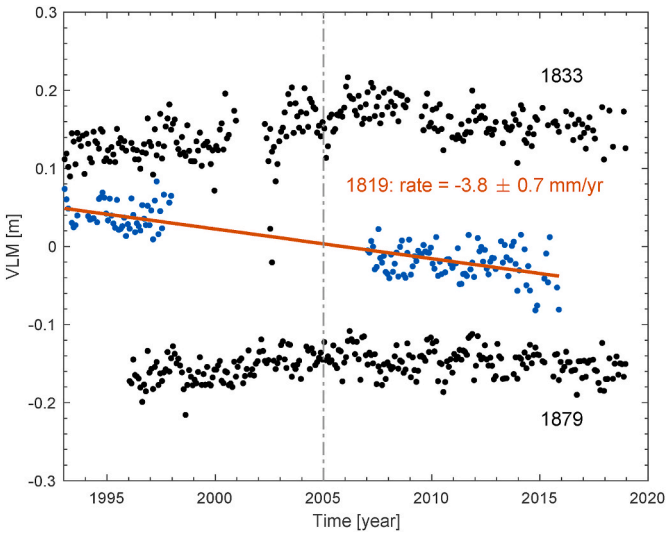

Fig. 12. VLM time series for sites 1833 (black dots), 1819 (blue dots) and 1879 (black dots). Red line is a linear fit to blue dots. (For interpretation of the references to color in this figure legend, the reader is referred to the Web version of this article.)

2021). For example, it has been reported that sediment compaction coupled with sediment accretion leads to land subsidence at an average rate of 15 mm/yr at the Yellow River Delta in China (Liu et al., 2021). It is likely that sediment compaction is also the driving process responsible for a major portion of the observed land subsidence since significant sediment accretion has been found around this site.

Site 1819 is also close (a few km) to a large area of peat swamp forest which has degraded around 15% in the period 1990–2015 for industrial use and urban development (Hoyt et al., 2020; Xu et al., 2018). Peatlands of the Baram system accumulated on alluvial sediments (Omar et al., 2022). Therefore, peatland degradation could enhance subsidence at site 1819 by intensified compaction resulted from increased stress due to drainage of peatland or infrastructural loading and organic matter decomposition (oxidation) as site 1819 and the peatland are connected by sandy layers along the shoreline. Hoogland et al. (2012) demonstrated that peat oxidation could result in land subsidence (~0.7 mm/yr) at locations without peat, although soils containing peat layers sink at a faster rate (up to 8 mm/yr).

7. Summary

We estimated coastal VLM time series using satellite altimetry and tide-gauge observations for 50 sites in Southeast Asia over the period of 1993–2020. We validated the VLM using GNSS observations at six sites and found that VLM estimates from the best correlated gridded satellite altimetry time series have a better agreement with GNSS observations than VLM estimates using along-track CCI coastal sea level time series. Our VLM results show various land behaviors (uplift, subsidence, a mix of uplift and subsidence), which are quantitatively or qualitatively consistent with previous observations from other sources. We inferred that the possible contributions of the VLM include inter- and post-seismic processes, groundwater extraction and sediment compaction. In addition to those major contributors to the VLM at tide-gauge sites, residual systematic errors in the satellite altimetry sea-level series, tide-gauge datum errors and differences in oceanographic conditions between onshore tide gauges and offshore satellite altimetry observations may also influence the VLM derived from combining satellite altimetry and tide-gauge observations. Despite these factors, we anticipate that this dataset will be useful for various scientific investigations, including studies on tectonics and sea level, as well as flood risk analyses and the development of associated mitigation strategies.

CRediT authorship contribution statement

Dongju Peng: Writing – original draft, Methodology, Investigation, Formal analysis, Conceptualization. **Grace Ng:** Writing – review & editing, Methodology, Investigation. **Lujia Feng:** Writing – review & editing, Investigation. **Anny Cazenave:** Writing – review & editing. **Emma M. Hill:** Writing – review & editing, Project administration, Funding acquisition.

Data availability statement

We obtained tide-gauge records from the Permanent Service for Mean Sea Level (PSMSL: https://psmsl.org/) and GNSS observations from the Nevada Geodetic Laboratory (http://geodesy.unr.edu/). Satellite altimetry sea-level products are distributed by the Copernicus Marine Environment Monitoring Service (CMEMS: https://marine.copernicus.eu/). The VLM time series for all the 50 sites estimated in this study are available at DR-NTU (data) https://doi.org/10.21979/N9/HODM0Y.

Funding

This research was supported by Singapore Ministry of Education Academic Research Fund Tier 3 (MOE, 2019-T3-1-004), and by the National Research Foundation Singapore under its NRF Investigatorship scheme (National Research Investigatorship Award No. NRF-NRFI05-2019-0009). This Research was also supported by the National Research Foundation, Singapore, and National Environment Agency, Singapore under the National Sea Level Programme Funding Initiative (Award No. USS-IF-2020-5).

Declaration of competing interest

The authors declare that they have no known competing financial interests or personal relationships that could have appeared to influence the work reported in this paper.

Acknowledgments

We thank the reviewers and editors for their valuable comments which helped to improve the manuscript. This work comprises Earth Observatory of Singapore contribution 627.

Appendix A. Supplementary data

Supplementary data to this article can be found online at https://doi.org/10.1016/j.srs.2024.100176.

Data availability

I have shared the link to my data.

References

Abidin, H.Z., Andreas, H., Gumilar, I., Fukuda, Y., Pohan, Y.E., Deguchi, T., 2011. Land subsidence of Jakarta (Indonesia) and its relation with urban development. Nat. Hazards 59 (3), 1753–1771.

Anandkumar, A., Vijith, H., Nagarajan, R., Jonathan, M., 2019. Evaluation of decadal shoreline changes in the coastal region of Miri, Sarawak, Malaysia. In: Coastal Management. Elsevier, pp. 95–119.

Arias, P., Bellouin, N., Coppola, E., Jones, R., Krinner, G., Marotzke, J., Naik, V., Palmer, M., Plattner, G.-K., Rogelj, J., 2021. Climate Change 2021: the Physical Science Basis. Contribution of Working Group14 I to the Sixth Assessment Report of the Intergovernmental Panel on Climate Change. Technical Summary.

Ballu, V., Bouin, M.-N., Siméoni, P., Crawford, W.C., Calmant, S., Boré, J.-M., Kanas, T., Pelletier, B., 2011. Comparing the role of absolute sea-level rise and vertical tectonic motions in coastal flooding, Torres Islands (Vanuatu). Proc. Natl. Acad. Sci. USA 108 (32), 13019–13022.

Becker, M., Papa, F., Karpytchev, M., Delebecque, C., Krien, Y., Khan, J.U., Ballu, V., Durand, F., Le Cozannet, G., Islam, A.S., 2020. Water level changes, subsidence, and sea level rise in the Ganges–Brahmaputra–Meghna delta. Proc. Natl. Acad. Sci. USA 117 (4), 1867–1876.

Benveniste, J., Birol, F., Calafat, F., Cazenave, A., Dieng, H., Gouzenes, Y., Legeais, J.F., Léger, F., Niño, F., Passaro, M., Schwatke, C., Shaw, A., 2020. Coastal sea level anomalies and associated trends from Jason satellite altimetry over 2002–2018. Sci. Data 7 (1), 357.

Birol, F., Léger, F., Passaro, M., Cazenave, A., Niño, F., Calafat, F.M., Shaw, A., Legeais, J.-F., Gouzenes, Y., Schwatke, C., 2021. The X-TRACK/ALES multi-mission processing system: new advances in altimetry towards the coast. Adv. Space Res. 67 (8), 2398–2415.

Blewitt, G., Hammond, W.C., Kreemer, C., 2018. Harnessing the GPS data explosion for interdisciplinary science. Eos 99 (10.1029), 485.

Bult, S.V., Le Bars, D., Haigh, I.D., Gerkema, T., 2024. The effect of the 18.6-year lunar nodal cycle on steric sea level changes. Geophys. Res. Lett. 51 (8), e2023GL106563.

Carrère, L., Lyard, F., 2003. Modeling the barotropic response of the global ocean to atmospheric wind and pressure forcing-comparisons with observations. Geophys. Res. Lett. 30 (6).

Cazenave, A., Dominh, K., Ponchaut, F., Soudarin, L., Cretaux, J., Le Provost, C., 1999. Sea level changes from Topex-Poseidon altimetry and tide gauges, and vertical crustal motions from DORIS. Geophys. Res. Lett. 26 (14), 2077–2080.

Cazenave, A., Gouzenes, Y., Birol, F., Leger, F., Passaro, M., Calafat, F.M., Shaw, A., Nino, F., Legeais, J.F., Oelsmann, J., 2022. Sea level along the world's coastlines can be measured by a network of virtual altimetry stations. Comm. Earth Environ. 3 (1), 1–9.

De Biasio, F., Baldin, G., Vignudelli, S., 2020. Revisiting vertical land motion and sea level trends in the Northeastern Adriatic Sea using satellite altimetry and tide gauge data. J. Mar. Sci. Eng. 8 (11), 949.

Dieng, H., Cazenave, A., Gouzenes, Y., Sow, B., 2021. Trends and inter-annual variability of altimetry-based coastal sea level in the Mediterranean Sea: comparison with tide gauges and models. Adv. Space Res. 68 (8), 3279–3290.

Din, A.H.M., Zulkifli, N.A., Hamden, M.H., Aris, W.A.W., 2019. Sea level trend over Malaysian seas from multi-mission satellite altimetry and vertical land motion corrected tidal data. Adv. Space Res. 63 (11), 3452–3472.
Fadil, A., Denys, P., Tenzer, R., Grenfell, H.R., Willis, P., 2013. New Zealand 20th century sea level rise: Resolving the vertical land motion using space geodetic and geological data. J. Geophys. Res. Ocean 118 (11), 6076–6091.
Featherstone, W., Penna, N., Filmer, M., Williams, S., 2015. Nonlinear subsidence at Fremantle, a long-recording tide gauge in the Southern Hemisphere. J. Geophys. Res.: Oceans 120 (10), 7004–7014.
Feng, L., Hill, E.M., Banerjee, P., Hermawan, I., Tsang, L.L., Natawidjaja, D.H., Suwargadi, B.W., Sieh, K., 2015. A unified GPS-based earthquake catalog for the Sumatran plate boundary between 2002 and 2013. J. Geophys. Res. Solid Earth 120 (5), 3566–3598.
Fenoglio-Marc, L., Schöne, T., Illigner, J., Becker, M., Manurung, P., Khafid, 2012. Sea level change and vertical motion from satellite altimetry, tide gauges and GPS in the Indonesian region. Mar. Geodesy 35 (Suppl. 1), 137–150.
Hamling, I.J., Wright, T.J., Hreinsdóttir, S., Wallace, L.M., 2022. A snapshot of New Zealand's dynamic deformation field from Envisat InSAR and GNSS observations between 2003 and 2011. Geophys. Res. Lett. 49 (2).
Hammond, W.C., Blewitt, G., Kreemer, C., Nerem, R.S., 2021. GPS imaging of global vertical land motion for studies of sea level rise. J. Geophys. Res. Solid Earth 126 (7), e2021JB022355.
Han, W., Webster, P.J., 2002. Forcing mechanisms of sea level interannual variability in the Bay of Bengal. J. Phys. Oceanogr. 32 (1), 216–239.
Herrera-García, G., Ezquerro, P., Tomás, R., Béjar-Pizarro, M., López-Vinielles, J., Rossi, M., Mateos, R.M., Carreón-Freyre, D., Lambert, J., Teatini, P., 2021. Mapping the global threat of land subsidence. Science 371 (6524), 34–36.
Holgate, S.J., Matthews, A., Woodworth, P.L., Rickards, L.J., Tamisiea, M.E., Bradshaw, E., Foden, P.R., Gordon, K.M., Jevrejeva, S., Pugh, J., 2013. New data systems and products at the permanent service for mean sea level. J. Coast Res. 29 (3), 493–504.
Hoogland, T., Van den Akker, J., Brus, D., 2012. Modeling the subsidence of peat soils in the Dutch coastal area. Geoderma 171, 92–97.
Hoyt, A.M., Chaussard, E., Seppalainen, S.S., Harvey, C.F., 2020. Widespread subsidence and carbon emissions across Southeast Asian peatlands. Nat. Geosci. 13 (6), 435–440.
Hutchison, C.S., 2005. Geology of North-West Borneo: Sarawak, Brunei and Sabah. Elsevier.
Iz, H.B., Shum, C.K., Yang, T.Y., 2020. Conflation of satellite altimetry and tide gauge records at coast. J. Geod. Sci. 10 (1), 62–68.
Kuo, C.Y., Shum, C.K., Braun, A., Mitrovica, J.X., 2004. Vertical crustal motion determined by satellite altimetry and tide gauge data in Fennoscandia. Geophys. Res. Lett. 31 (1).
Li, L., Switzer, A.D., Wang, Y., Chan, C.-H., Qiu, Q., Weiss, R., 2018. A modest 0.5-m rise in sea level will double the tsunami hazard in Macau. Sci. Adv. 4 (8), eaat1180.
Liu, Y., Liu, J., Xia, X., Bi, H., Huang, H., Ding, R., Zhao, L., 2021. Land subsidence of the Yellow River Delta in China driven by river sediment compaction. Sci. Total Environ. 750, 142165.
Minderhoud, P., Erkens, G., Pham, V., Bui, V.T., Erban, L., Kooi, H., Stouthamer, E., 2017. Impacts of 25 years of groundwater extraction on subsidence in the Mekong delta, Vietnam. Environ. Res. Lett. 12 (6), 064006.
Mohamed Rashidi, A.H., Jamal, M.H., Hassan, M.Z., Mohd Sendek, S.S., Mohd Sopie, S. L., Abd Hamid, M.R., 2021. Coastal structures as beach erosion control and sea level rise adaptation in Malaysia: a review. Water 13 (13), 1741.
Nan, F., Xue, H., Yu, F., 2015. Kuroshio intrusion into the south China sea: a review. Prog. Oceanogr. 137, 314–333.
Nicholls, R.J., Lincke, D., Hinkel, J., Brown, S., Vafeidis, A.T., Meyssignac, B., Hanson, S. E., Merkens, J.-L., Fang, J., 2021. A global analysis of subsidence, relative sea-level change and coastal flood exposure. Nat. Clim. Change 11 (4), 338–342.
Oelsmann, J., Marcos, M., Passaro, M., Sanchez, L., Dettmering, D., Dangendorf, S., Seitz, F., 2024. Regional variations in relative sea-level changes influenced by nonlinear vertical land motion. Nat. Geosci. 17 (2), 137–144. https://doi.org/10.1038/s41561-023-01357-2.
Oelsmann, J., Passaro, M., Dettmering, D., Schwatke, C., Sánchez, L., Seitz, F., 2021. The zone of influence: matching sea level variability from coastal altimetry and tide gauges for vertical land motion estimation. Ocean Sci. 17 (1), 35–57. https://doi.org/10.5194/os-17-35-2021.
Omar, M.S., Ifandi, E., Sukri, R.S., Kalaitzidis, S., Christanis, K., Lai, D.T.C., Bashir, S., Tsikouras, B., 2022. Peatlands in Southeast Asia: a comprehensive geological review. Earth Sci. Rev. 232, 104149.
Peng, D., Hill, E.M., Meltzner, A.J., Switzer, A.D., 2019. Tide gauge records show that the 18.61-year nodal tidal cycle can change high water levels by up to 30 cm. J. Geophys. Res.: Oceans 124 (1), 736–749.
Petersen, M., Harmsen, S., Mueller, C., Haller, K., Dewey, J., Luco, N., Crone, A., Lidke, D., Rukstales, K., 2007. Documentation for the Southeast Asia Seismic Hazard Maps, vol. 30, p. 2007. *Administrative Report September*.
Pfeffer, J., Allemand, P., 2016. The key role of vertical land motions in coastal sea level variations: a global synthesis of multisatellite altimetry, tide gauge data and GPS measurements. Earth Planet Sci. Lett. 439, 39–47. https://doi.org/10.1016/j.epsl.2016.01.027.
Phien-wej, N., Giao, P.H., Nutalaya, P., 2006. Land subsidence in bangkok, Thailand. Eng. geolo. 82 (4), 187–201.
Poitevin, C., Wöppelmann, G., Raucoules, D., Le Cozannet, G., Marcos, M., Testut, L., 2019. Vertical land motion and relative sea level changes along the coastline of Brest (France) from combined space-borne geodetic methods. Rem. Sens. Environ. 222, 275–285. https://doi.org/10.1016/j.rse.2018.12.035.
Qiu, Q., Moore, J.D., Barbot, S., Feng, L., Hill, E.M., 2018. Transient rheology of the Sumatran mantle wedge revealed by a decade of great earthquakes. Nat. Commun. 9 (1), 1–13.
Raucoules, D., Le Cozannet, G., Wöppelmann, G., De Michele, M., Gravelle, M., Daag, A., Marcos, M., 2013. High nonlinear urban ground motion in Manila (Philippines) from 1993 to 2010 observed by DInSAR: implications for sea-level measurement. Rem. Sens. Environ. 139, 386–397.
Reimann, L., Vafeidis, A.T., Brown, S., Hinkel, J., Tol, R.S., 2018. Mediterranean UNESCO World Heritage at risk from coastal flooding and erosion due to sea-level rise. Nat. Commun. 9 (1), 1–11.
Rezvani, M.-H., Watson, C.S., King, M.A., 2022. Vertical deformation and residual altimeter systematic errors around continental Australia inferred from a Kalman-based approach. J. Geodesy 96 (12), 96.
Rezvani, M.H., Watson, C.S., King, M.A., 2021. Estimating vertical land motion and residual altimeter systematic errors using a kalman-based approach. J. Geophys. Res.: Oceans 126 (6). https://doi.org/10.1029/2020jc017106.
Rezvani, M.H., Watson, C.S., King, M.A., 2024. Non-linear vertical land motion of coastal Chile and the Antarctic Peninsula inferred from combining satellite altimetry, tide gauge and GPS data. J. Geophys. Res. Solid Earth 129 (6), e2023JB028103.
Rodolfo, K.S., Siringan, F.P., 2006. Global sea-level rise is recognised, but flooding from anthropogenic land subsidence is ignored around northern Manila Bay, Philippines. Disasters 30 (1), 118–139.
Sansosti, E., Berardino, P., Bonano, M., Calò, F., Castaldo, R., Casu, F., Manunta, M., Manzo, M., Pepe, A., Pepe, S., 2014. How second generation SAR systems are impacting the analysis of ground deformation. Int. J. Appl. Earth Obs. Geoinf. 28, 1–11.
Santamaría-Gómez, A., 2019. SARI: interactive GNSS position time series analysis software. GPS Solut. 23 (2), 1–6.
Santamaría-Gómez, A., Gravelle, M., Collilieux, X., Guichard, M., Míguez, B.M., Tiphaneau, P., Wöppelmann, G., 2012. Mitigating the effects of vertical land motion in tide gauge records using a state-of-the-art GPS velocity field. Global Planet. Change 98, 6–17.
Santamaría-Gómez, A., Gravelle, M., Wöppelmann, G., 2014. Long-term vertical land motion from double-differenced tide gauge and satellite altimetry data. J. Geodesy 88 (3), 207–222.
Satirapod, C., Trisirisatayawong, I., Fleitout, L., Garaud, J., Simons, W., 2013. Vertical motions in Thailand after the 2004 Sumatra–Andaman Earthquake from GPS observations and its geophysical modelling. Adv. Space Res. 51 (8), 1565–1571.
Schöne, T., Illigner, J., Manurung, P., Subarya, C., Zech, C., Galas, R., 2011. GPS-controlled tide gauges in Indonesia–a German contribution to Indonesia's Tsunami Early Warning System. Nat. Hazards Earth Syst. Sci. 11 (3), 731–740.
Shirzaei, M., Freymueller, J., Törnqvist, T.E., Galloway, D.L., Dura, T., Minderhoud, P.S., 2021. Measuring, modelling and projecting coastal land subsidence. Nat. Rev. Earth Environ. 2 (1), 40–58.
Simons, W.J., Naeije, M.C., Brown, B.E., Niemnil, S., Pradit, S., Thongtham, N., Mustafar, M.A., Towatana, P., Darnsawasdi, R., Yucharoen, M., 2019. Vertical motion of Phuket Island (1994–2018) due to the Sumatra-Andaman mega-thrust earthquake cycle: impact on sea-level and consequences for coral reefs. Mar. Geol. 414, 92–102.
Sreenivas, P., Gnanaseelan, C., Prasad, K., 2012. Influence of El Niño and Indian ocean dipole on sea level variability in the bay of bengal. Global Planet. Change 80, 215–225.
Taburet, G., Sanchez-Roman, A., Ballarotta, M., Pujol, M.-I., Legeais, J.-F., Fournier, F., Faugere, Y., Dibarboure, G., 2019. Duacs DT2018: 25 years of reprocessed sea level altimetry products. Ocean Sci. 15 (5), 1207–1224. https://doi.org/10.5194/os-15-1207-2019.
Tay, C., Lindsey, E.O., Chin, S.T., McCaughey, J.W., Bekaert, D., Nguyen, M., Hua, H., Manipon, G., Karim, M., Horton, B.P., 2022. Sea-level rise from land subsidence in major coastal cities. Nat. Sustain. 1–9.
Trisirisatayawong, I., Naeije, M., Simons, W., Fenoglio-Marc, L., 2011. Sea level change in the Gulf of Thailand from GPS-corrected tide gauge data and multi-satellite altimetry. Global Planet. Change 76 (3–4), 137–151.
Vu, D., Yamada, T., Ishidaira, H., 2018. Assessing the impact of sea level rise due to climate change on seawater intrusion in Mekong Delta, Vietnam. Water Sci. Technol. 77 (6), 1632–1639.
Watson, C.S., White, N.J., Church, J.A., King, M.A., Burgette, R.J., Legresy, B., 2015. Unabated global mean sea-level rise over the satellite altimeter era. Nat. Clim. Change 5 (6), 565–568. https://doi.org/10.1038/nclimate2635.
Watson, P.J., 2019. An assessment of the utility of satellite altimetry and tide gauge data (ALT-TG) as a proxy for estimating vertical land motion. J. Coast Res. 35 (6), 1131–1144.
Woodworth, P.L., Melet, A., Marcos, M., Ray, R.D., Wöppelmann, G., Sasaki, Y.N., Cirano, M., Hibbert, A., Huthnance, J.M., Monserrat, S., 2019. Forcing factors affecting sea level changes at the coast. Surv. Geophys. 40 (6), 1351–1397.
Wöppelmann, G., Marcos, M., 2012. Coastal sea level rise in southern Europe and the nonclimate contribution of vertical land motion. J. Geophys. Res. Ocean 117 (C1).
Wöppelmann, G., Marcos, M., 2016. Vertical land motion as a key to understanding sea level change and variability. Rev. Geophys. 54 (1), 64–92.
Xu, J., Morris, P.J., Liu, J., Holden, J., 2018. PEATMAP: refining estimates of global peatland distribution based on a meta-analysis. Catena 160, 134–140.